OCEAN OPTICS XIII, Eds. Steven G. Ackleson and Robert Frouin,
22-25 October 1996, Halifax, Nova Scotia, Canada, SPIE Volume 2963, Bellingham, WA, USA, 906 pp., 1997

Optical spectral signatures of marine sediments

Walton E. McBride III
Planning Systems Inc., 115 Christian Lane, Slidell, LA 70458, USA
e-mail: <walt_mcbride@psislidell.com>

Vladimir I. Haltrin, Clark D. Kennedy, and Alan D. Weidemann
Naval Research Laboratory, Ocean Sciences Branch, Code 7331
Stennis Space Center, MS 39529-5004, USA. e-mail: <haltrin@nrlssc.navy.mil>

ABSTRACT

In studying light and image transfer in coastal waters the influence of bottom reflection is as significant as scattering and absorption phenomena. In these cases a knowledge of the reflective properties of different types of bottoms is very important. At present, little is known about these properties. We present results of experimental spectral measurements of different kinds of sedimental material such as sands and clays, both major components of coastal water bottoms.

We have determined the spectral index of refraction from measurements of the optical spectral signatures of various clays and sands, as they represent the most common bottom components found in coastal waters. The measured optical spectral signatures and the associated complex indexes of refraction are presented. This preliminary study should provide insight on improving the inverse problem algorithm for extracting the spectral index of refraction. This spectral information can then be used as input into radiative transfer models which include the ocean bottom.

Keywords: reflectance, refraction index, optical constants, optical signatures, ocean sediments.

1. INTRODUCTION

Our overall motivation is to be able to characterize bottom properties with a wavelength- dependent spectrum of dielectric permittivities to be used as input into an underwater propagation model. Equivalently, we would like to obtain a rough estimate for the complex index of refraction of particular samples as a function of wavelength from the simplest possible assumptions and measurements about the reflective properties of typical bottom sediments. From these acquired spectral values for the real and imaginary parts of the index of refraction, the reflective properties of a sample can be calculated as a function of the angle of incidence for a particular wavelength, a characterization which can easily be input into the numerical simulation of a theoretical model. Because of the simple experimental design our initial goal is to obtain reflectances within 20% of their measured values over a range of incidence angles varying from normal to 30 degrees.

For each wavelength in the spectrum, there are two unknowns, *i.e.*, the real and imaginary part of the index of refraction, often referred to as the optical constants. Methods exist [1] to deal with the inverse problem of determining these quantities for flat surfaces, such as reflectometry and ellipsometry. Specular reflectance measurements were performed in order to try to infer the complex index of refraction as a function of wavelength. In the next section, we describe the algorithm which we used to address this inverse problem.

2. INVERSION ALGORITHM

In order to quantify the real and imaginary parts of the complex index of refraction, two different measurements must be made. For specular reflectance measurements, there are two variables which can be used in tandem: the source polarization (perpendicular or transverse to the plane of incidence) and the angle of incidence (from 0 to 90 degrees).

In an effort to obtain an estimate of the complex index of refraction as a function of wavelength, the following simplifying assumption was made: only single reflections from the air/sample interface contribute to the intensity at the spectral radiometer. In effect, for a particular angle of incidence, only those facets at the sample surface which specularly reflect light into the spectral radiometer aperture are assumed to contribute. Multiple reflections from facets at different orientations to each other are not considered. For rough surfaces such as clays and sands, it is expected that some modification of the simple theory involving the Fresnel intensity reflection coefficients for flat surfaces will be needed.

2.1. Fresnel intensity reflection coefficients

Given the angle of incidence θ_i with respect to the boundary normal between two dielectrics, the Fresnel intensity coefficients for the parallel and transverse polarizations at the specular reflection angle are respectively given by [2]:

$$R_p = \left| \frac{\sqrt{m^2 - \sin^2\theta_i} - m^2\cos\theta_i}{\sqrt{m^2 - \sin^2\theta_i} + m^2\cos\theta_i} \right|^2 \quad and \quad R_t = \left| \frac{\sqrt{m^2 - \sin^2\theta_i} - \cos\theta_i}{\sqrt{m^2 - \sin^2\theta_i} + \cos\theta_i} \right|^2 \tag{1}$$

where the complex index of refraction $m = n_r + in_i$. For normal incidence the reflectance is the same for both polarizations, effectively resulting in only one measurement. An incidence angle of 30 degrees was also chosen, giving two more measurements depending on the source polarization.

2.2. Algorithm description

Our simple algorithm makes use of all three measurements in a search for the minimum of a sum of absolute differences for each wavelength. The differences in this sum are between the corresponding measured and theoretically-predicted reflectances. Let R_{00}^{data} be the reflectance value at normal incidence (same for both polarizations) and $R_{30\,p}^{data}$ and R_{30t}^{data} be the reflectance values for parallel and transverse polarizations at 30 degrees. Then, for each wavelength in the measured reflectance spectra, the inversion algorithm proceeds as follows.

Loops are performed over a user-given range of values for n_r and n_i. For each (n_r, n_i) pair, the Fresnel intensity reflection coefficients R_{00}^{theory}, $R_{30\,p}^{theory}$ and R_{30t}^{theory} are calculated and differenced with their measured counterparts. The sum of the three absolute differences, $abs\left(R_{00}^{theory} - R_{00}^{data}\right) + abs\left(R_{30\,p}^{theory} - R_{30\,p}^{data}\right) + abs\left(R_{30t}^{theory} - R_{30t}^{data}\right)$, is then minimized while keeping track of the (n_r, n_i) pair which resulted in the minimum for each wavelength.

The range over which both n_r and n_i are searched is determined by the user, as well as the discretization of these variables. Discretization was chosen to be a grid of 1000 by 1000 possible values for n_r and n_i. For the first pass, values of n_r and n_i between 0.0 and 3.0 are allowed since we have no initial idea of the range of these variables. The grid described above enables the algorithm to find the values to at least the second decimal place while narrowing the ranges in n_r and n_i. In order to further zoom in on the minimum, two additional passes are performed with a 100 by 100 grid of total width equal to twice the previous increments in n_r and n_i and centered on the inferred values of n_r and n_i from the previous pass.

Problems were anticipated when $n_i << n_r$ due to the statistical nature of the reflectance measurements. Realistically, only when n_i is comparable in size to n_r can the inversion algorithm be expected to predict n_i with any confidence. In order to get an idea of the inversion capabilities of the algorithm when the reflectance data is known exactly, synthetic data was generated.

2.3. Synthetic data for algorithm test

Before the algorithm was applied to experimental data, its performance was tested against synthetic reflectance data generated over a wavelength spectrum between 450 and 800 nm. The data was generated from assumed Gaussian functional forms for both the real and imaginary parts of the index of refraction:

$$n_r(\lambda) = 2.0 - e^{-\left(\frac{\lambda - 450.0}{150.0}\right)^2} \quad and \quad n_i(\lambda) = .5e^{-\left(\frac{\lambda - 450.0}{150.0}\right)^2}. \tag{2}$$

The functional form for n_i was chosen so as to span a wide range of values, from .5 at 450 nm to about 2.2×10^{-3} at 800 nm, as small values for that parameter were expected.

The Fresnel intensity reflection coefficients were then calculated for each wavelength to obtain the theoretically-predicted reflectance spectra for normal incidence as well as for the two polarizations at 30 degrees. These reflectance spectra were used as "experimental" data input to the inversion algorithm which then finds the (n_r, n_i) pair that best matches.

Figure 1 below is an illustration of the assumed functional shapes for n_r and n_i and the inferred values (asterisks) for both parameters. Figure 2 shows the original synthetic reflectances (R_{30t}, R_{00} and $R_{30\,p}$ from top to bottom) computed directly from the assumed Gaussian functional forms for n_r and n_i and the reflectances at 11 equally spaced points computed from the inferred values of n_r and n_i. The percentage difference between the two reflectances is under 1% for all points on each of the three curves.

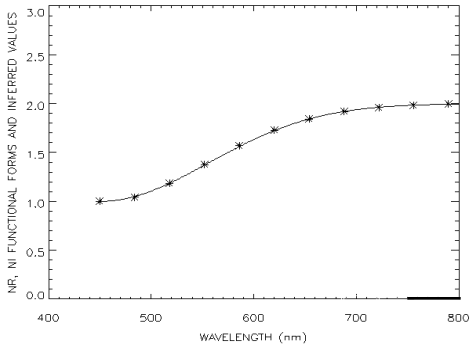

Figure 1: Inferred and synthetic values of index of refraction.

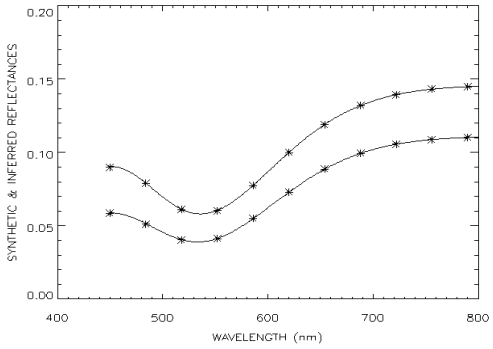

Figure 2: Comparison between inferred and synthetic reflectances

Satisfied with the ability of the algorithm to reliably predict the (n_r, n_i) spectra which generated the synthetic data, we applied the algorithm to the experimental data we collected.

3. EXPERIMENTAL REFLECTANCE MEASUREMENTS

Experimental data was gathered in air with a xenon arc lamp as the light source. The output of the lamp was defocused at a 2.5 cm aperture. The image of the aperture was projected through a second lens to form a 10 cm circular spot (at normal incidence) at 34 cm from the lens. This produced a diffuse image of the aperture which would be the same as that produced from a point source at 45 cm from the surface which has been stopped down to 12.2 degrees. The polarizer was mounted between the projecting lens and the target surface. The detector was a CCD-based spectral radiometer (ASD). The foreoptic of the radiometer had a 1 degree acceptance angle and is mounted at 53 cm from the target. The detected spot diameter was about 1 cm near the center of the projected aperture image.

Three different samples were used for measurement purposes: a backyard orange-brown clay affectionately coined "Waltonian" clay by our group and two types of sand collected from coastal areas, referred to simply as gray sand and brown sand. Calibration of the measured reflectance spectra was performed with the help of a gray reflector with known reflective properties. All inferred values for n_r and n_i are with respect to air.

4. INVERSION ALGORITHM APPLIED TO EXPERIMENTAL DATA

As with the synthetic data, 11 points were picked from the three experimental reflectance curves in order to save computing time. Because each reflectance curve represents an average over only 10 spectrometer samples, enough "noise" in these curves is present to adversely effect the inversion algorithm.

Figure 3a below shows the values of n_r and n_i inferred from the experimental reflectance curves in Figure 3b for Waltonian clay (top is R_{30t}, middle is R_{00} and (almost overlapping) bottom is R_{30p}). As can be seen, the inversion algorithm predicts values for n_i only below 500 nm. Predictions for n_i over the rest of the wavelength band appear to be meaningless when compared to the more gradual falloff in Figure 1. Interestingly enough, the inferred values for n_i below 500 nm are comparable in size to n_r , a criterion we needed for the inversion algorithm to predict values of n_i with any confidence. The thin lines in Figure 3b connect the 11 reflectance points corresponding to the inferred (n_r, n_i) pairs. Error percentages between corresponding reflectances are presented later in Section 5.

For materials such as sands, however, simple Fresnel theory had to be modified. As can be seen from the experimental data in Figures 4b and 5b, two trends occur which Fresnel theory is incapable of explaining: the top curve is now R_{00} followed by R_{30t} and R_{30p} while the gap between the latter two is much narrower than the gap predicted by Fresnel theory for the inferred (n_r, n_i) values. We have therefore applied two modifications to the inversion algorithm in the case of sands.

The first modification involves the fall-off of the unpolairzed reflected intensity at 30 degrees for both polarizations as compared to simple Fresnel theory. As shown in Ref. [3], the unpolarized reflectance is almost constant from normal to 30 degrees incidence over the n_r and n_i ranges of interest here. The inversion algorithm candidate reflectances at 30 degrees were therefore divided by the ratio of the unpolarized reflectances at normal and 30 degrees incidence, $2R_{00}^{data}/(R_{30p}^{data} + R_{30t}^{data})$,before performing the sum of the three absolute differences, as explained in Section 2.2. The second modification is discussed in Section 5.

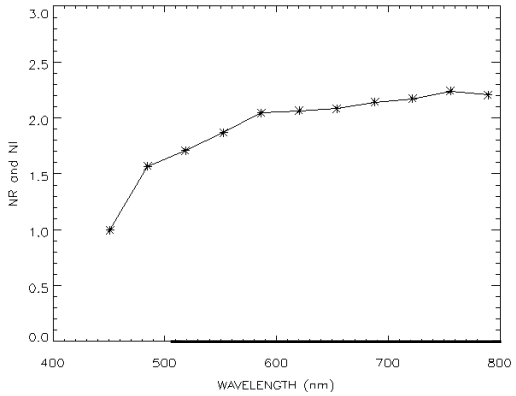

Figure 3a. Inferred values of n_r and n_i for Waltonian clay

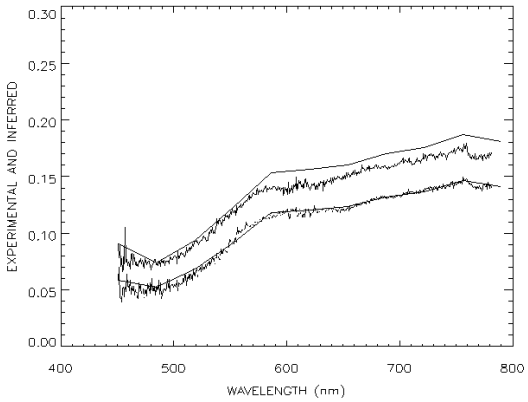

Figure 3b. Experimental and inferred reflectances for Waltonian clay

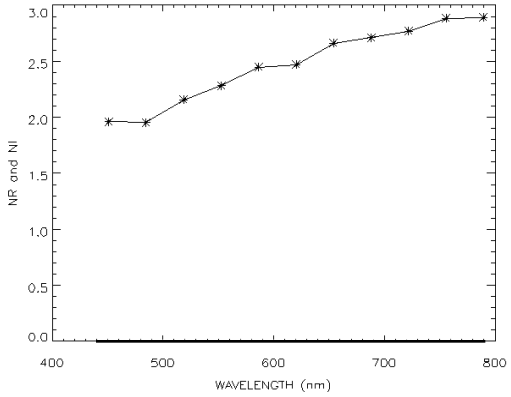

Figure 4a. Inferred values of n_r and n_i for brown sand

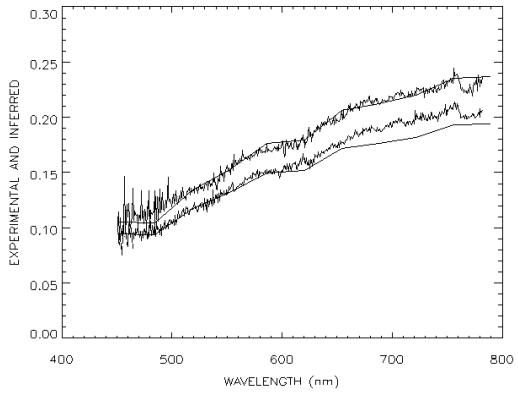

Figure 4b. Experimental and inferred reflectances for brown sand

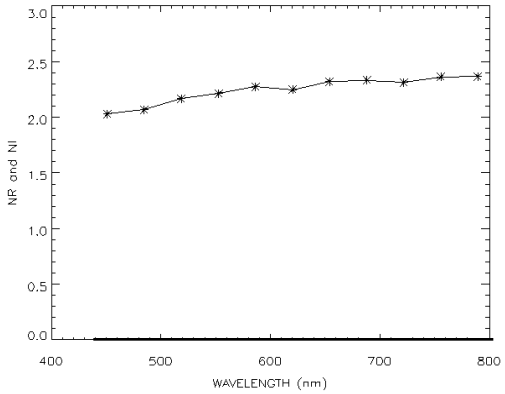

Figure 5a. Inferred values of n_r and n_i for gray sand

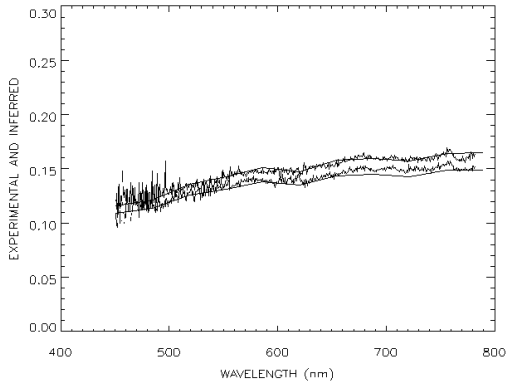

Figure 5b. Experimental and inferred reflectances for gray sand

Although values for n_i were predicted for a few wavelengths in the Waltonian clay case, disappointing results can be seen for both types of sand, as shown in Figures 4a and 5a. Nevertheless, values for n_r were obtained. Whether the absence of any predictions for n_i is due to the noise in the reflectance curves, the smallness of n_i or the inapplicability of Fresnel theory altogether needs to be investigated.

5. REFLECTANCE PLOTS AS A FUNCTION OF INCIDENCE ANGLE

Once the optical constants of each sample were obtained as a function of wavelength, reflectance plots as a function of incidence angle were produced over the visible spectrum . Figures 6a, 7a and 8a show such predictions at a wavelength of 600 nm for the three samples in our experiment (top for perpendicular, middle for unpolarized and bottom for parallel), while figures 6b, 7b, and 8b show the percentage error between experimental and inferred reflectances discussed in Section 4 (light for R_{30p}, medium for R_{00}, and dark for R_{30t}). In all cases there is excellent agreement for R_{00}. Overall, our original goal of obtaining reflectances within 20% of their experimental values seems to be achievable.

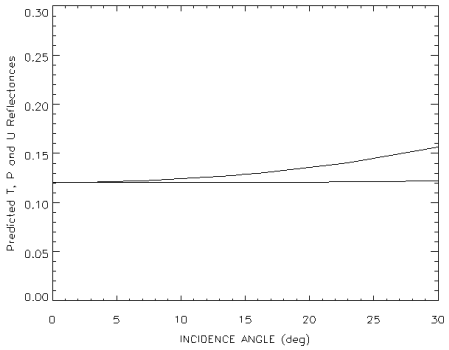

Figure 6a. Reflectances at 600 nm for Waltonian clay

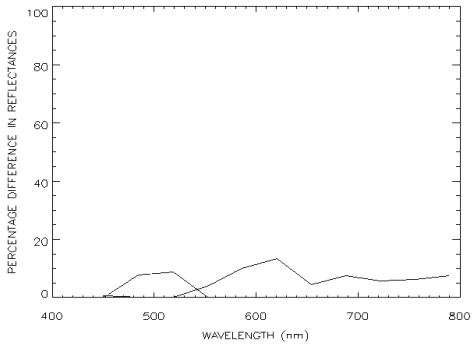

Figure 6b. Percentage error between reflectances for Waltonian clay

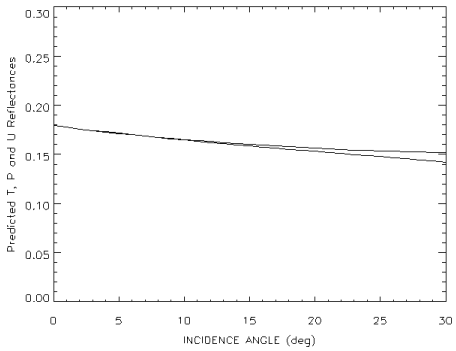

Figure 7a. Reflectances at 600 nm for brown sand

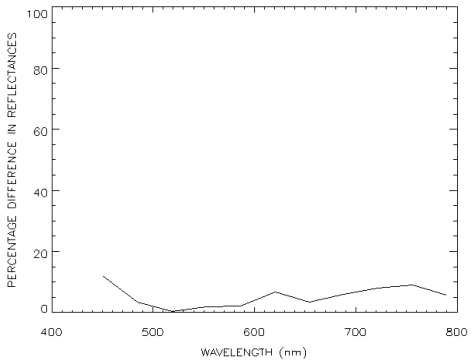

Figure 7b. Percentage error between reflectances for brown sand

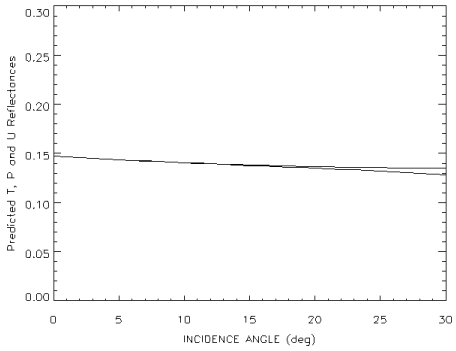

Figure 8a. Reflectances at 600 nm for gray sand

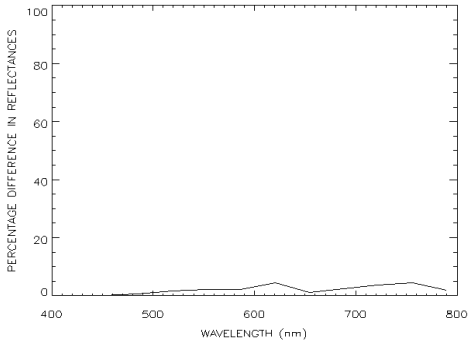

Figure 8b. Percentage error between reflectances for gray sand

Except for Waltonian clay where the inversion algorithm was run without modifications, the percentage error between experimental and inferred reflectances at 30 degrees was calculated by adjusting the gap between the curves corresponding to different polarizations. Because of the large inferred values for n_r in sands, the gap predicted by Fresnel

theory is much wider than the one gathered from experimental data. A second modification to simple Fresnel theory was therefore necessary.

Because of its constancy over the incidence angles of interest to our study, the unpolarized reflectance at 30 degrees was used as a reference point from which the modification was made. Let *gapdata* be the ratio of the transverse to unpolarized reflectances from experimental data at 30 degrees for the middle wavelength of 600 nm, while *gaptheory* is the corresponding quantity derived from Fresnel theory. Then the theoretical transverse and parallel reflectances were modified as follows:

$$R_{30t}^{modified} = \frac{R_{30t}}{falloff}\left(\frac{gapdata}{gaptheory}\right) \quad and \quad R_{30p}^{modified} = \frac{R_{30p}}{falloff}\left(\frac{2-gapdata}{2-gaptheory}\right) \tag{3}$$

where *falloff* represents the first modification discussed previously involving the fall-off of reflected intensity as the incidence angle increases, $2R_{00}^{data}/(R_{30p}^{data}+R_{30t}^{data})$. In order to produce Figures 7a and 7b for sands, the following interpolations were performed:

$$R_t = R_t^{theory}\frac{R_t^{fact}(\theta)}{fall(\theta)} \quad and \quad R_p = R_p^{theory}\frac{R_p^{fact}(\theta)}{fall(\theta)} \tag{4}$$

where

$$fall(\theta) = 1.0 + (falloff - 1.0)F(\theta), \tag{5}$$

$$R_t^{fact} = 1.0 + \left(\frac{gapdata}{gaptheory} - 1.0\right)F^2(\theta) \quad and \quad R_p^{fact} = 1.0 + \left(\frac{2-gapdata}{2-gaptheory} - 1.0\right)F^2(\theta) \tag{6}$$

and

$$F(\theta) = \frac{\sin\theta}{\sin 30^0}. \tag{7}$$

The result of the two modifications can be seen in figures 7a and 8a for brown and gray sands, respectively. Notice how the unpolarized reflectance shows a fall-off as the angle of incidence increases from normal to 30 degrees. The second modification is also apparent as the gap between the two polarizations is much narrower than predicted by simple Fresnel theory for the range of values of n_r encountered in our study.

6. CONCLUSIONS

We have used an inversion algorithm involving simple Fresnel reflection theory to determine the spectral index of refraction from specular reflectance measurements of clay. It was found that two modifications to simple theory were necessary for sands in order to reproduce the experimental reflectance curves from the inferred optical constants.

Because our interest in the complex index of refraction stems from our theoretical modeling requirements, our next priority is to build a small database of the optical constants for the most common types of marine sediment. In that regard, more automated instrumentation would be preferred and a more thorough investigation of the reason behind the disappointing results for n_i will be undertaken. As work progresses, a search for more efficient and accurate methods to find n_r and n_i such as neural network and simulated annealing will be undertaken.

Water tank experiments are also needed so that the marine sediments are in their natural environments. Some simple way will be found to illuminate a submerged surface and to obtain n_r and n_i relative to the index of refraction of water.

7. ACKNOWLEDGMENTS

The authors wish to thank continuing support at the Naval Research Laboratory through the Littoral Optical Environment (LOE 6640-06) and Optical Oceanography (OO 73-5051-05) programs. This article represents NRL contribution NRL/PP/7331–96–0010. The authors would like to take this opportunity to thank Richard Ray for his assistance.

8. REFERENCES

1. L. Ward, Ed., *The Optical Constants of Bulk Materials and Films*, Institute of Physics Publishing, Bristol and Philadelphia, PA, p. 350, 1994.
2. D. V. Sivukhin, *General Course in Physics, Vol. 4: Optics* (in Russian), Moscow, Nauka, p. 406, 1985.
3. E. Palick, *Handbook of Optical Constants of Solids*, Academic Press, New York, N.Y., p.72, Figure 1, 1985.